Direct numerical simulation–based Reynolds-averaged closure for bubble-induced turbulence

Tian Ma,[1,2,*] Claudio Santarelli,[2] Thomas Ziegenhein,[1] Dirk Lucas,[1] and Jochen Fröhlich[2]
[1]*Helmholtz-Zentrum Dresden-Rossendorf, Institute of Fluid Dynamics, 01328 Dresden, Germany*
[2]*Technische Universität Dresden, Institute of Fluid Mechanics, 01062 Dresden, Germany*
(Received 10 November 2016; published 1 March 2017)

Budgets of the turbulent kinetic energy from direct numerical simulations (DNSs) of disperse bubbly channel flows are used to develop a model for bubble-induced turbulence in the Euler-Euler Reynolds-averaged framework. First, an appropriate time scale is selected. Second, links between the unclosed terms in the transport equations of the turbulence quantities and the DNS data for small bubbles are established. Third, a suitably chosen iterative procedure employing the full Reynolds-averaged model provides suitable coefficients for the closure of the terms resulting from bubble-induced turbulence while largely removing the influence of others. At the same time these results validate the closure, exhibiting very good agreement with the DNS and better performance than the standard closures. The model is now ready for use and can be employed in practical Euler-Euler simulations.

DOI: 10.1103/PhysRevFluids.2.034301

I. INTRODUCTION

Turbulence and multiphase flows are two of the most challenging topics in fluid mechanics and when combined they pose a formidable challenge, even in the dilute dispersed regime [1]. This particularly holds for flows laden with disperse bubbles as these have low momentum on their own, resulting in very strong coupling to the liquid phase. Bubbly flows can be investigated numerically by various approaches at different levels of detail. For large-scale simulations the Euler-Euler (EE) approach [2] coupled with steady or unsteady Reynolds-averaged Navier-Stokes (RANS) modeling is the only viable framework. Here the bubble-induced turbulence (BIT) of the liquid phase is one of the most important and delicate effects to model. It was represented by an algebraic viscosity in the work of [3]. Another algebraic modeling of BIT based on potential theory [4] turned out to be too simplistic [5]. Later on, BIT was considered by supplementing single-phase two-equation turbulence models with specific source terms [6–12]. A different approach based on single-phase simulation without resolving bubbles was proposed in Ref. [13].

The present work starts from the equations for two-phase flows rigorously derived in Ref. [14]. These equations are based on a single-phase representation and take the influence of bubbles into account by including additional interfacial terms in the balance equations both for k, the turbulent kinetic energy (TKE), and ε, the dissipation rate. When supplementing the unclosed terms in these equations with adequate models they constitute an appropriate framework for RANS modeling of bubbly flows. Due to the lack of reliable data for individual terms, however, the models used in the literature are mostly based on *ad hoc* physical considerations.

Recently, direct numerical simulations (DNS) have become available to shed light on the details of the physics involved [15–19]. Ilić [20] performed DNS to evaluate each term in the TKE budget for up to eight bubbles. She demonstrated that the gain of TKE is mainly caused by the interfacial term, while the contribution of the production term is negligible. Erdogan and Wörner [21] extended this work to larger bubble Reynolds numbers Re_p, showing that the TKE of the liquid phase increases with Re_p. Further DNS data with substantially higher Reynolds number, realistic density ratio, and large domains have recently been provided in Refs. [22,23].

*tian.ma@hzdr.de

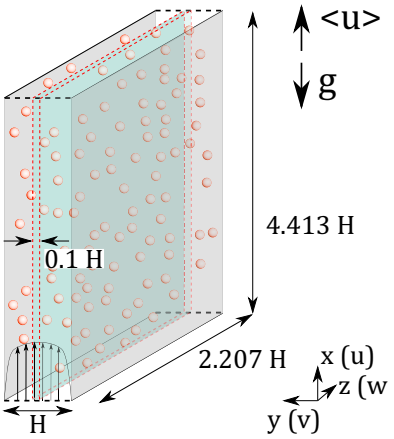

FIG. 1. Schematic representation of the DNS configuration (not to scale). The marked region indicates the location where the spatial energy spectra were computed.

In the present paper we propose a closure for the BIT terms in an EE RANS model on the basis of DNS data. Two main issues are addressed: the time scale of the BIT source in the dissipation equation and the coefficients in the BIT source expressions of the two-equation RANS model used. The resulting model is then validated by computing the same cases with the EE model. Beyond the resulting model itself the paper also furnishes a systematic procedure that is of general use.

II. DIRECT NUMERICAL SIMULATION DATABASE

To serve the present purpose, the DNS data have to provide information about all relevant processes, in particular the interfacial effects. This requires that the bubble geometry is resolved, in contrast to the point-particle approach, occasionally addressed also as DNS of a multiphase flow [1]. In Refs. [22,23], bubble-resolving DNS with many thousands of bubbles at low Eötvös number were conducted. In this case, a spherical shape can be safely assumed. Compared to other simulations of this type [20,21], these simulations exhibit substantial differences so that they are close to applications: turbulent background flow, contaminated fluid, realistic density ratio (1000 instead of 2), higher bubble Reynolds number, much larger domain, and much larger number of bubbles. The technically involved numerical procedure to evaluate the TKE budget used as an input for the present work was presented in detail in Ref. [24].

The DNSs were conducted for upward flow in a rectangular channel, with periodicity in the streamwise (x) and spanwise (z) directions. The size of the domain is $L_x \times L_y \times L_z = 4.41H \times H \times 2.21H$, where H is the distance of the walls (Fig. 1). The bulk velocity U_b was kept constant by instantaneously adjusting a volume force, equivalent to a pressure gradient, thus imposing the bulk Reynolds number $\mathrm{Re}_b = U_b H/\nu$, where ν is the kinematic viscosity of the liquid. The DNS data used in this work were obtained for three monodisperse cases and one bidisperse case with half the void fraction consisting of smaller bubbles and the other half of larger bubbles, all at the same bulk Reynolds number $\mathrm{Re}_b = 5263$. Table I provides an overview of all cases with the labels of the cited references. The data available cover statistical moments of first and second order for liquid and bubbles.

While the DNSs were performed using a nondimensional set of parameters, the EE RANS closure proposed in the present work is related to the bubble diameter d_p, with the corresponding simulations conducted in dimensional units. For this reason the above setup is converted to a dimensional form using the contaminated air-water system as an example. Based on the discussion in Ref. [25] the pivoting element is chosen to be the equality of the Archimedes number $\mathrm{Ar} = |\pi_\rho - 1| g d_p^3/\nu^2$, with π_ρ denoting the bubble-to-liquid density ratio. Keeping Ar the same as in the DNSs and using all the

TABLE I. Parameters of the DNS cases used for the present modeling. The labels Sm (smaller) and La (larger) designate different bubble sizes and when used with the bidisperse case indicate averaging over the fraction of smaller and larger bubbles, respectively. Here N_p is the number of bubbles, α the void fraction, d_p the particle diameter, and Ar the Archimedes number. The values of Re_p, the particle Reynolds number (based on d_p and the relative velocity u_r), and C_D, the drag coefficient, are results of the simulations.

Parameter \ Case	SmMany	SmFew	LaMany	BiDisp(Sm)	BiDisp(La)
N_p	2880	384	913	1440	546
α	2.14%	0.29%	2.14%	1.07%	1.07%
d_p/H	0.052	0.052	0.076	0.052	0.076
Ar	38171	38171	114528	38171	114528
Re_p	236	268	475	234	464
C_D	0.89	0.71	0.67	0.93	0.70

other physical dimensional parameters in the definition of Ar yields $d_p = 1.456$ mm for the smaller bubbles and $d_p = 2.127$ mm for the larger bubbles. The ratio d_p/H in Table I then results in the extensions $123.6 \times 28.0 \times 61.8$ mm^3 of the channel.

III. ENERGY SPECTRA AND TIME SCALES

In the first step energy spectra are determined on the basis of the DNS data to define an appropriate time scale for BIT. In bubbly flows, Lance and Bataille [26] were the first to find a power-law scaling with a slope of about $-8/3$ and provide a scaling argument yielding -3, which was confirmed by later studies [17,27–32]. The calculation of spectra in a bubble-laden flow is delicate, as the phase boundaries tend to interrupt the signal. Here an approach is proposed that is ideally suited for DNS of dilute disperse flows. It is based on a spatial selection of signals without the presence of bubbles and the feature of periodic boundary conditions employed by the simulation anyway. For the case SmMany, liquid velocity was recorded along grid lines in the spanwise direction within the center region $0.45H < y < 0.55H$ (Fig. 1), sufficiently thin to warrant statistical equivalence of these lines. For each line, data were recorded whenever the line was free of bubbles, resulting in 50 000 one-dimensional data sets. The velocity values were taken on the staggered grid of the simulation, without being interpolated as in Ref. [17]. As the range in z covers the entire domain, the periodic boundary conditions employed for the simulation result in periodic signals, so the data can be Fourier transformed without windowing. This was performed for each velocity component with subsequent averaging over the computed spectra. Figure 2(a) shows the resulting energy spectra. They all have a similar shape and exhibit three different ranges: a low-wave-number range reflecting the large-scale turbulence, a medium range with decay rate around -3 for wavelengths $\lambda = 0.001$–0.003 m, and a higher-wave-number range with stronger decay similar to [26].

The characteristic length scale for BIT is still a subject of debate in the literature. Different length scales on the order of d_p have been proposed, located in the -3 subrange [27,31], which supports the present result. A comparison between the different studies is complicated by the use of different methods to calculate the spectra, but the cited works, as well as the present one show that d_p is included in the typical -3 subrange for BIT. Hence, from a modeling point of view, d_p is chosen as a starting point for a BIT length scale.

In a similar manner, the choice of a suitable time scale τ is based on temporal spectra. Here these are obtained in two steps. According to [29,31], the spatial spectra in the streamwise direction are the same as those in the spanwise direction. Second, Taylor's hypothesis is employed to convert streamwise spatial spectra into temporal spectra, resulting in Fig. 2(b). Two candidates for a time scale, $(\sqrt{k}/d_p)^{-1}$ [10] and $(u_r/d_p)^{-1}$ [8], are included along with the single-phase RANS time scale $(\varepsilon/k)^{-1}$ used in Ref. [9] for comparison. The result in Fig. 2(b) suggests that $\tau = d_p/u_r$ is a good

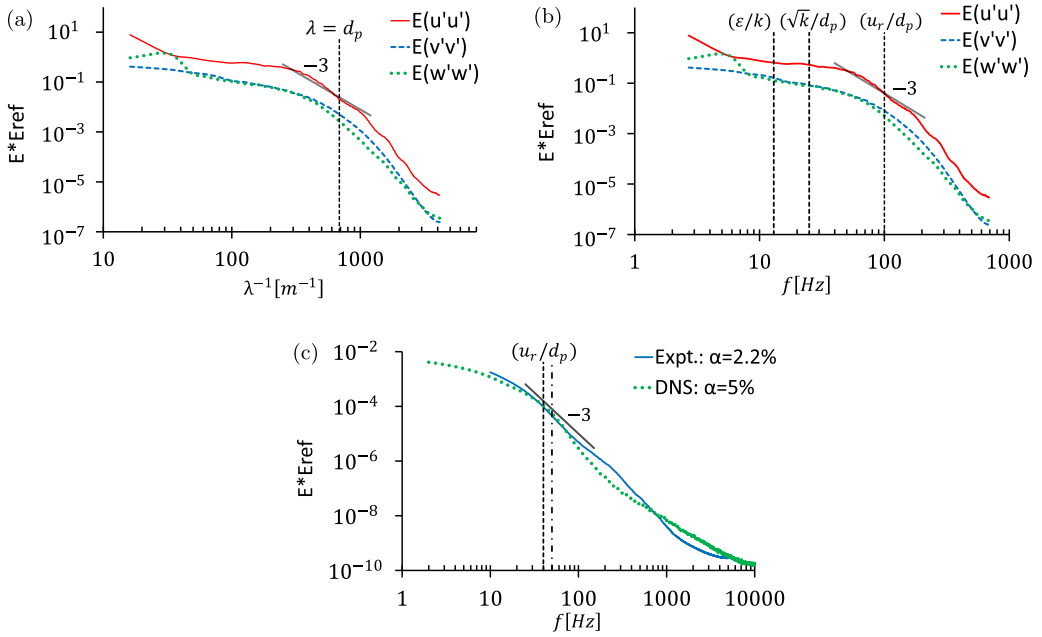

FIG. 2. Spectra of liquid velocity from DNS and experiment of bubbly flow, with vertical lines illustrating the reference scales indicated. (a) Spatial spectra from DNS SmMany. (b) Temporal spectra from DNS SmMany. (c) Temporal spectra from the experiment of [27] and DNS of [17], labeled Expt. and DNS, respectively. Here - - - - - - - denotes u_r/d_p from experiment and – · – · – denotes u_r/d_p from DNS.

starting point for a time scale characterizing BIT since this frequency is in the typical −3 BIT range, while the others are not. This is consistent with the requirement that a model for ε has to account for the turbulence scales as well as for the different length scales and the fast energy decay due to the presence of bubbles [33]. Figure 2(c) confirms the suitability of d_p/u_r by the experiment of [27] with $u_r/d_p \sim 40$ Hz and the DNS of [17] with $u_r/d_p \sim 50$ Hz.

IV. TURBULENCE MODELING

For incompressible two-phase flow, the governing equations of the Euler-Euler approach are

$$\frac{\partial(\alpha^K \rho^K)}{\partial t} + \nabla \cdot (\alpha^K \rho^K \boldsymbol{u}^K) = 0, \tag{1}$$

$$\frac{D(\alpha^K \rho^K \boldsymbol{u}^K)}{Dt} = -\nabla \cdot (\alpha^K \mu^K \boldsymbol{S}^K) - \alpha^K \nabla p + \alpha^K \rho^K \boldsymbol{g} + \boldsymbol{M}^K - \nabla \cdot \left(\alpha^K \boldsymbol{\tau}_t^K\right), \tag{2}$$

where all quantities are mean values. The superscript K denotes the phases (L denotes liquid and G gas), with μ, $\boldsymbol{u}$, and $\boldsymbol{S}$ being the molecular viscosity, the mean velocity, and the mean strain rate tensor, respectively. The unresolved stress tensor $\boldsymbol{\tau}_t$ and the sum of all interfacial forces $\boldsymbol{M}$ acting on phase K have to be modeled. Established models for the different nondrag interfacial forces are employed here, based on an extensive literature study: the model of [34] for lift, the model of [35] for the wall force, and the model of [36] for turbulent dispersion. Details on how the various coefficients of the models were determined are given in Sec. V below.

According to [14], the TKE k of the liquid phase in a turbulent bubbly flow is governed by the budget equation

$$\frac{D\overline{\phi}k}{Dt} = \Pi_k + D_k + \varepsilon_k \underbrace{-\frac{1}{\rho}\overline{p'_L u'_{L,i} n_i I} + \frac{1}{\rho}\overline{\tau'_{L,ij} u'_{L,i} n_j I}}_{S_k}, \tag{3}$$

with ϕ an indicator for the liquid phase and the overbar denoting statistical averaging. The production term Π_k, the diffusion term D_k, and the dissipation term ε_k are the same as with single-phase flow [37]. The term S_k represents the interfacial energy transfer between bubbles and liquid and is an additional source term created by the presence of the bubbles. Here p'_L, $u'_{L,i}$, and $\tau'_{L,ij}$ are the fluctuations of pressure, the ith velocity component, and the stress tensor at the liquid side of the phase boundary, respectively. Finally, n_i is the normal vector at the phase boundary directed toward the gas phase and I is the interfacial area concentration with $\partial\phi/\partial x_i = -I n_i$.

To close the single-phase terms in Eq. (3) the shear stress transport (SST) model [38] is employed, supplemented with a source term S_k^{RANS} accounting for production of BIT

$$\frac{D(\alpha^L \rho^L k)}{Dt} = \Pi_k^{\mathrm{RANS}} + D_k^{\mathrm{RANS}} \underbrace{-\alpha^L C_\mu \rho^L \omega k}_{\varepsilon_k^{\mathrm{RANS}}} \underbrace{+C_I \boldsymbol{F}_D \cdot (\boldsymbol{u}^G - \boldsymbol{u}^L)}_{S_k^{\mathrm{RANS}}}, \tag{4}$$

where k and ω are given without the upper index L for simplicity. Further modeling now focuses on the interfacial term S_k, which in the considered cases is balanced by the dissipation [24], so these two terms are the dominant ones in the center region of the channel, which is the focus of the present work. The total energy input by the bubbles is equal to the work done by the buoyancy force $\boldsymbol{F}_B \cdot \boldsymbol{u}^G$. In a steady state, this is equal to the work done by the drag $\boldsymbol{F}_D \cdot \boldsymbol{u}^G$, which can be decomposed into $\boldsymbol{F}_D \cdot \boldsymbol{u}^L + \boldsymbol{F}_D \cdot (\boldsymbol{u}^G - \boldsymbol{u}^L)$. The equation for the mean kinetic energy of the liquid is obtained from (2) by multiplying with the liquid mean velocity $\boldsymbol{u}^L$. The contribution $\boldsymbol{F}_D \cdot \boldsymbol{u}^L$ to the term $\boldsymbol{M}^L \cdot \boldsymbol{u}^L$ in the mean kinetic energy equation drives the mean flow, so the energy converted into turbulence is

$$S_k^{\mathrm{RANS}} = C_I \boldsymbol{F}_D \cdot (\boldsymbol{u}^G - \boldsymbol{u}^L), \tag{5}$$

with the parameter $C_I \leqslant 1$ and $\boldsymbol{F}_D = \frac{3}{4d_p} C_D \rho^L \alpha^G |\boldsymbol{u}^G - \boldsymbol{u}^L| (\boldsymbol{u}^G - \boldsymbol{u}^L)$. Figure 3 compares the expression $\boldsymbol{F}_D \cdot (\boldsymbol{u}^G - \boldsymbol{u}^L)$, based on *a priori* tests, to S_k from (3). Remarkably, the shape of these curves is very similar. Hence, adjusting the coefficient C_I bears the potential of successful modeling.

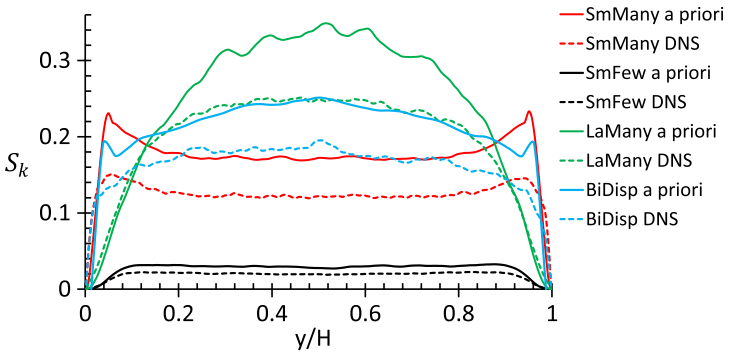

FIG. 3. Comparison between the interfacial term S_k according to (3) and the *a priori* evaluation of S_k^{RANS}/C_I (5) for all cases, both normalized with U_b^3/H.

The ω equation of the two-phase SST model is

$$\frac{D(\alpha^L\rho^L\omega)}{Dt} = D_\omega^{\mathrm{RANS}} + \Pi_\omega^{\mathrm{RANS}} + C_\omega^{\mathrm{RANS}} \underbrace{-\alpha^L C_{\omega D}\rho^L\omega^2}_{\varepsilon_\omega^{\mathrm{RANS}}} \underbrace{+\left(\frac{1}{C_\mu k}S_\varepsilon^{\mathrm{RANS}} - \frac{\omega}{k}S_k^{\mathrm{RANS}}\right)}_{S_\omega^{\mathrm{RANS}}}, \tag{6}$$

where all single-phase terms are given in Ref. [38]. The term

$$S_\varepsilon^{\mathrm{RANS}} = C_\varepsilon \frac{S_k^{\mathrm{RANS}}}{\tau} \tag{7}$$

in Eq. (6) is the BIT source in the ε equation transformed to an equivalent source in the ω equation using the same time scale τ, with C_ε a model parameter. In single-phase flow $\tau = k/\varepsilon$ represents the large-scale eddy turnover time for shear-induced turbulence, but this is far away from the physics of BIT [Fig. 2(b)]. An essential step now is to replace this time scale with $\tau = d_p/u_r$ characterizing BIT according to Sec. III for use in the following.

V. MODEL PARAMETERS FOR THE DIFFERENT CASES

Euler-Euler RANS simulations were run in the same domain as the DNSs and discretized with $56 \times 60 \times 51$ grid points in the x, y, and z directions, respectively. Boundary conditions were identical to those of the DNS.

Based on the promising results of Fig. 3, the idea now is to determine the coefficients C_I and C_ε in Eqs. (5) and (7) for each DNS data set, which later on should reveal the general trend. If, however, the relative velocity or the void fraction is different, the BIT model cannot be assessed.

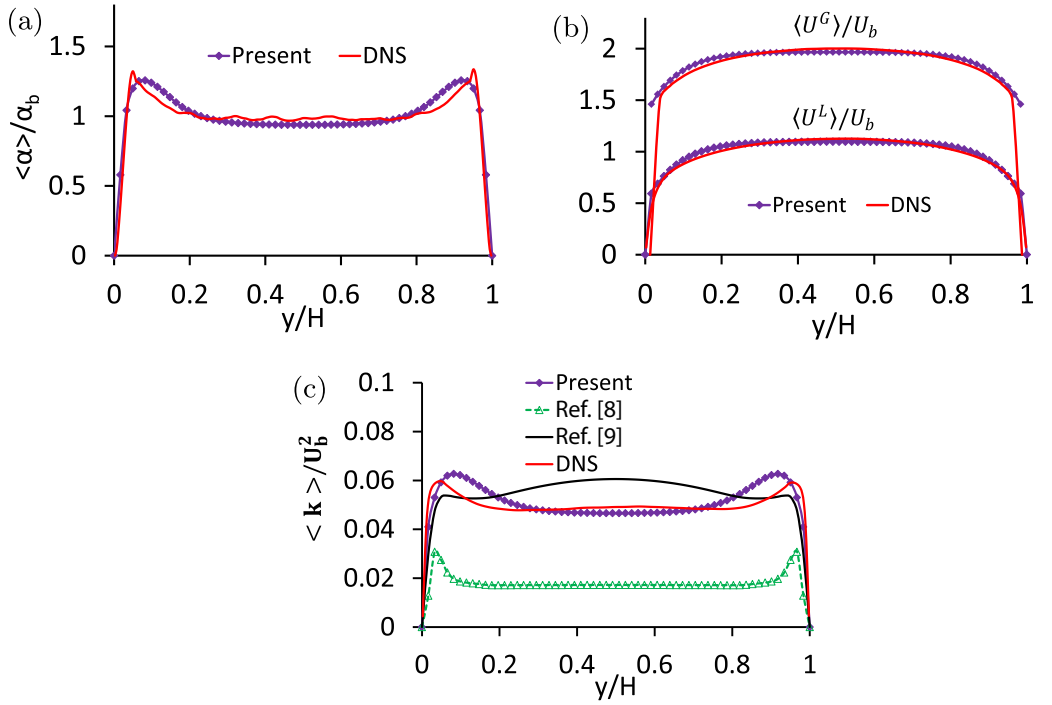

FIG. 4. One-point statistics from the present EE RANS model and DNS data for SmMany. (a) Gas void fraction. (b) Liquid streamwise velocity and gas streamwise velocity. (c) Liquid TKE and comparison with standard models.

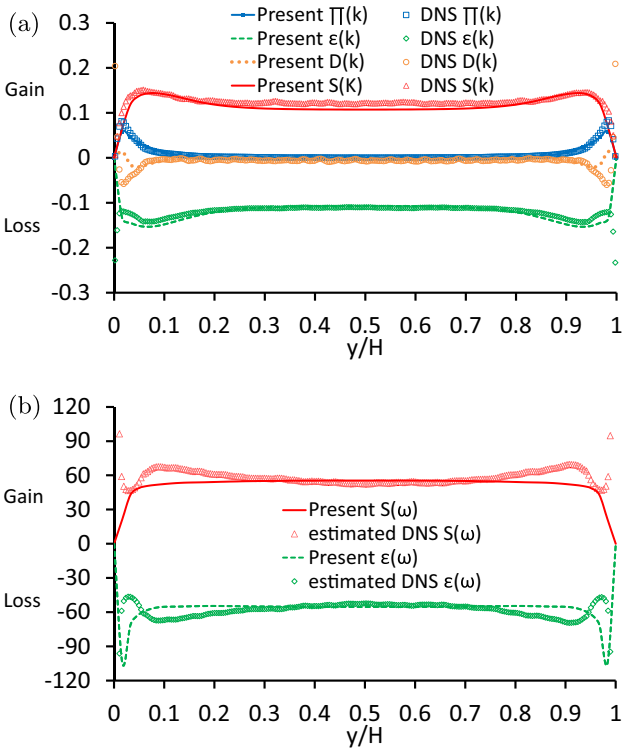

FIG. 5. Comparison of the present EE RANS model with the DNS data for the case of SmMany for (a) the k budget with all terms normalized by U_b^3/H and (b) the ω budget with all terms normalized by U_b^2/H^2.

Hence, a prerequisite is that the uncertainty created by the other submodels is removed as much as possible. To accomplish this, the drag coefficient was determined from the DNS data directly, i.e., from $u_r = |\boldsymbol{u}^G - \boldsymbol{u}^L|$. Then an iterative process was carried out by running EE RANS simulations simultaneously optimizing C_I, C_ε, and the lift coefficient C_L, while the other interfacial forces models were employed as they are. It turns out that the resulting value of $C_L = 0.06$ indeed yields the correct void fraction distribution [Fig. 4(a)]. The resulting values of $C_I = 0.64$ and $C_\varepsilon = 0.27$ provide very good matches of the DNS data for SmMany (Figs. 4 and 5). Here Fig. 4(b) shows the mean liquid and gas velocity obtained with these parameters. Both velocity profiles fit the DNS data very well. As expected, with C_D based on the DNS data, excellent agreement is obtained for the gas velocity. The TKE of the liquid phase is largely augmented due to bubbles in SmMany compared to the same situation without bubbles [22]. This is very well reproduced by the present EE RANS data in the channel remote from the walls. The performance of the model is substantially better than with the models from [8,9] under exactly the same conditions [Fig. 4(c)]. The budgets for k and ω are shown in Fig. 5. The originality of this process is that the targets of the iteration are not

TABLE II. Values of C_I, C_ε, and C_L obtained by the iterative process for all cases.

Parameter \ Case	SmMany	SmFew	LaMany	BiDisp(Sm)	BiDisp(La)
C_I	0.64	0.66	0.75	0.64	0.75
C_ε	0.27	0.15	0.2	0.27	0.2
C_L	0.06	0.0055	−0.03	0.08	−0.04

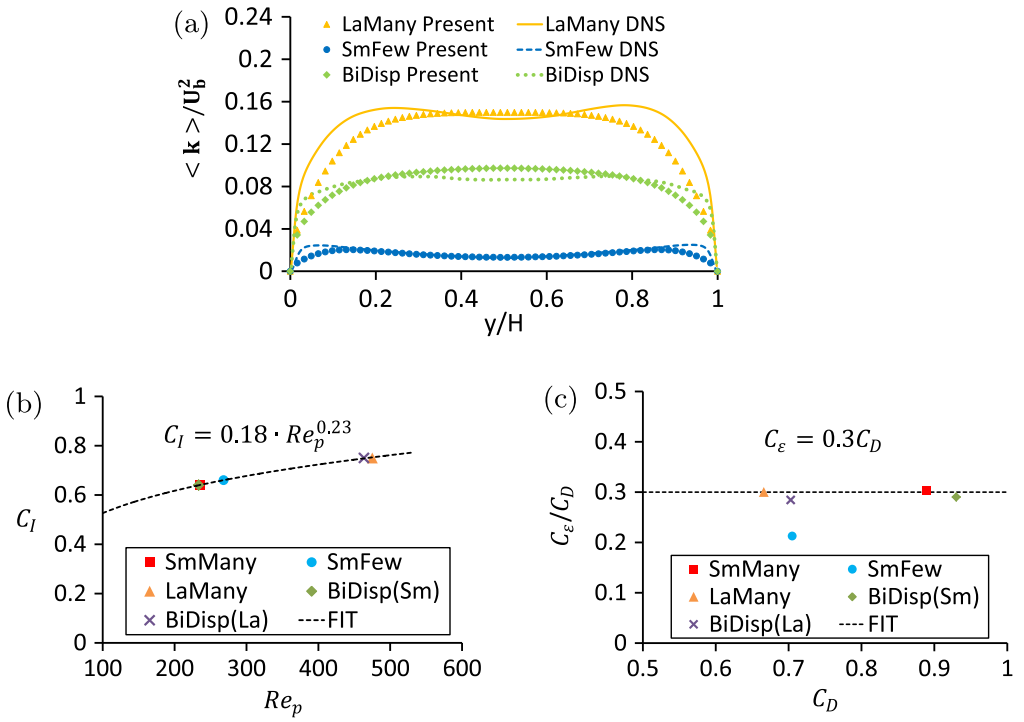

FIG. 6. (a) Comparison of k from simulations with the present model to DNS data for LaMany, SmFew, and BiDisp. (b) Values of C_I as a function of Re_p for all cases considered. The dashed line shows the fit. (c) Values of C_ε / C_D as a function of C_D for all cases considered. The dashed line shows the fit.

statistics of the mean flow but rather the values of the particular terms to be closed, resulting directly or indirectly from the DNS data, such as ε_k, S_k, ε_ω, and S_ω.

The target is defined in the core region of the channel, since matching this is a prerequisite to all modeling. Figure 5(a) shows that in the region the k equation (3) reduces to $0 \approx \varepsilon_k + S_k$, with both terms available from the DNS. For ω, however, no budget is available from the DNS data, but again $0 \approx \varepsilon_\omega + S_\omega$ in the center for the same reasons as with the k equation. Hence, ε_ω has to be determined indirectly from the DNS data. For this purpose, it is represented here by the expression for $\varepsilon_\omega^{\mathrm{RANS}}$ from (6), where α^L, ε, and k are determined by the DNS data

$$\varepsilon_\omega = -\alpha^L_{\mathrm{DNS}} C_{\omega D,2}\, \rho^L (\omega_{\mathrm{DNS}})^2, \quad \omega_{\mathrm{DNS}} = \frac{\varepsilon_{\mathrm{DNS}}}{C_\mu k_{\mathrm{DNS}}}, \tag{8}$$

using the standard coefficients $C_{\omega D,2} = 0.0828$ and $C_\mu = 0.09$ [38]. The same procedure is then employed for the other three bubble-laden cases, yielding the corresponding values of C_I, C_ε, and C_L (Table II), each achieving good agreement for the TKE [Fig. 6(a)] and the other terms (shown in Ref. [39]).

VI. MODEL FOR BUBBLE-INDUCED TURBULENCE

The final step is to propose a general model for the BIT terms. Based on the previous experience, this is done by providing a functional relation for the coefficients C_I and C_ε. The importance of Re_p for BIT and the observation in Ref. [21] that the TKE increases with Re_p for the same number of bubbles suggest to model C_I as a function of Re_p. The couples of the discrete values of C_I and Re_p are displayed in Fig. 6(b). For the case BiDisp, two data points are plotted for the smaller bubbles and the larger bubbles, respectively, with the assumption that the contributions from the two bubble sizes sum up to the total contribution. Obviously, C_I increases with Re_p. This supports the

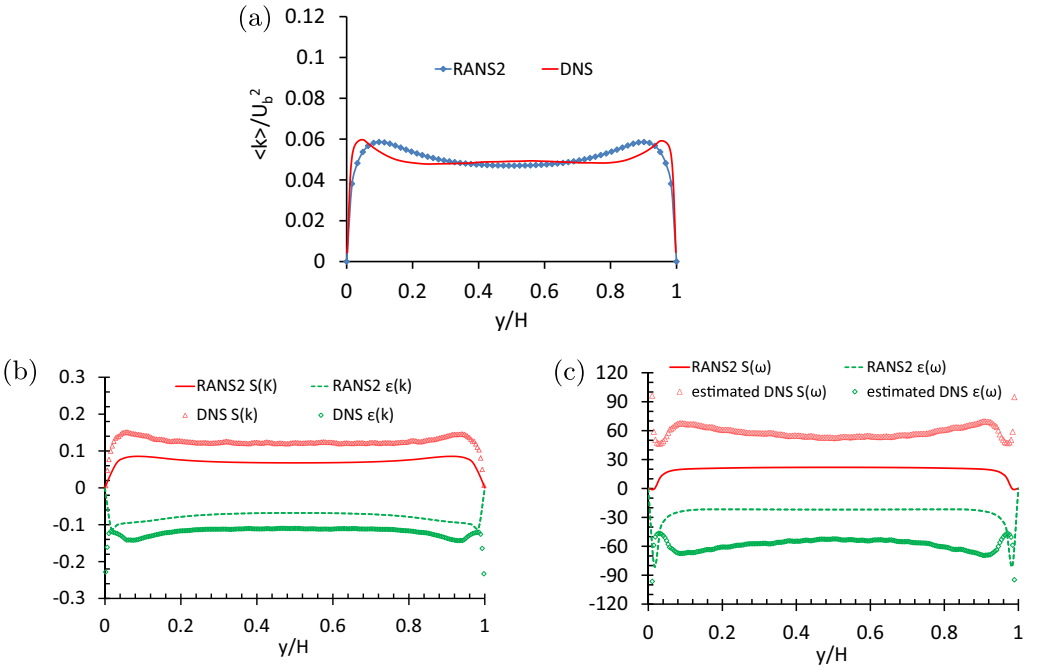

FIG. 7. Comparison of the simulation RANS2 ($C_I = 0.4$ and $C_\varepsilon = 0.17$) with DNS data for the case of SmMany for (a) liquid TKE, (b) the k budget normalized by U_b^3/H, and (c) the ω budget normalized by U_b^2/H^2.

hypothesis that bubbles with larger Re_p have stronger wake effects than bubbles with small Re_p and for even smaller Re_p the wake eventually disappears [40]. Hence, an Re_p-dependent expression for C_I seems suitable for S_k^{RANS}. Curve fitting of C_I by a power law [Fig. 6(b)] yields

$$S_k^{\mathrm{RANS}} = \underbrace{\min\left(0.18\,\mathrm{Re}_p^{0.23}, 1\right)}_{C_I} \boldsymbol{F}_D(\boldsymbol{u}^G - \boldsymbol{u}^L). \tag{9}$$

Here $C_I \leqslant 1$ is imposed to fulfill the energy balance discussed regarding (5).

The value of C_ε could be formulated as a function of $S_\varepsilon^{\mathrm{RANS}}$, of the BIT time scale, or of the BIT length scale, depending on the problem considered. Inspired by Riboux *et al.* [29], who found the characteristic length scale of BIT being related to d_p and the drag coefficient, the values of C_ε are plotted over C_D in Fig. 6(c). The relation $C_\varepsilon = 0.3C_D$ provides a very good match for the data points, except in the case of SmFew. This may be due to the very low void fraction (0.29%), so the influence of the background flow in this case is not negligible. Hence, the following closure is proposed:

$$S_\varepsilon^{\mathrm{RANS}} = \underbrace{0.3C_D}_{C_\varepsilon} \frac{S_k^{\mathrm{RANS}}}{\tau}, \tag{10}$$

with $\tau = d_p/u_r$.

VII. CONCLUSION

Equations (9) and (10) constitute a proposal for closing the BIT terms in a typical RANS model. This closure employs Re_p and C_D, which are available in any EE RANS simulation.

Using DNS data with iterations to obtain term-by-term match in the model equations avoids pitfalls of *ad hoc* models targeting the TKE only, as illustrated in Fig. 7. In a simulation labeled

RANS2 for the situation of SmMany, the values $C_I = 0.4$ and $C_\varepsilon = 0.17$ were employed instead of the values in Table II. The result for k fits well, but is related to an underprediction of the source terms in both the k and ω equations. This can yield further errors and does not solve the modeling problem. The present approach is exempt from this issue. This procedure can be employed in a similar way to well-resolved DNSs of many deformable bubbles at higher Reynolds number once these are available. The difference between the present proposal for C_I and the corresponding values of C_n in Ref. [24] are due to the fact that in Ref. [24] a slightly different procedure to evaluate the relative velocity was employed and that a kind of *a priori* test for the BIT term in the k equation was conducted, while here the complete EE RANS model as a whole is addressed.

The proposed BIT model is ready for use now. The procedure can as well be employed for any similar two-equation RANS model. As such, the model is valid for small bubbles in contaminated fluid, which is highly relevant for practical applications. Further tests should focus on the performance of the model over a wider range of bubble Reynolds numbers and in more complex flow fields.

ACKNOWLEDGMENTS

T.M. would like to acknowledge Andrea Prosperetti for an inspiring discussion about BIT during a workshop on bubbly flows. The data used in Fig. 2(c) were made available by Ivo Roghair. The authors also thank Yixiang Liao, Friederike Gauß, and Pavel Apanasevich for their enlightening suggestions. Partial funding was provided by the Helmholtz-Alliance LIMTECH, Project No. A5.

[1] S. Balachandar and J. K. Eaton, Turbulent dispersed multiphase flow, Annu. Rev. Fluid Mech. **42**, 111 (2010).
[2] M. Ishii and T. Hibiki, *Thermo-Fluid Dynamics of Two-Phase Flow* (Springer, Berlin, 2006).
[3] Y. Sato, M. Sadatomi, and K. Sekoguchi, Momentum and heat transfer in two-phase bubble flow—I. Theory, Int. J. Multiphase Flow **7**, 167 (1981).
[4] A. Biesheuvel and L. van Wijngaarden, Two-phase flow equations for a dilute dispersion of gas bubbles in liquid, J. Fluid Mech. **148**, 301 (1984).
[5] F. Risso and K. Ellingsen, Velocity fluctuations in a homogeneous dilute dispersion of high-Reynolds-number rising bubbles, J. Fluid Mech. **453**, 395 (2002).
[6] M. L. de Bertodano, R. T. Lahey, and O. C. Jones, Development of a k-ε model for bubbly two-phase flow, J. Fluids Eng. **116**, 128 (1994).
[7] C. Morel, Turbulence modeling and first numerical simulations in turbulent two-phase flows, in: 11th International Symposium on Turbulent Shear Flows, Grenoble, 1997.
[8] A. A. Troshko and Y. A. Hassan, A two-equation turbulence model of turbulent bubbly flows, Int. J. Multiphase Flow **27**, 1965 (2001).
[9] M. S. Politano, P. M. Carrica, and J. Converti, A model for turbulent polydisperse two-phase flow in vertical channels, Int. J. Multiphase Flow **29**, 1153 (2003).
[10] R. Rzehak and E. Krepper, CFD modeling of bubble-induced turbulence, Int. J. Multiphase Flow **55**, 138 (2013).
[11] M. Colombo and M. Fairweather, Multiphase turbulence in bubbly flows: RANS simulations, Int. J. Multiphase Flow **77**, 222 (2015).
[12] A. S. M. A. Islam, N. A. Adoo, and D. J. Bergstrom, Prediction of mono-disperse gas-liquid turbulent flow in a vertical pipe, Int. J. Multiphase Flow **85**, 236 (2016).
[13] G. Riboux, D. Legendre, and F. Risso, A model of bubble-induced turbulence based on large-scale wake interactions, J. Fluid Mech. **719**, 362 (2013).
[14] I. Kataoka and A. Serizawa, Basic equations of turbulence in gas-liquid two-phase flow, Int. J. Multiphase Flow **15**, 843 (1989).
[15] B. Bunner and G. Tryggvason, Effect of bubble deformation on the stability and properties of bubbly flows, J. Fluid Mech. **495**, 77118 (2003).

[16] I. A. Bolotnov, K. E. Jansen, D. A. Drew, A. A. Oberai, R. T. Lahey, and M. Z. Podowski, Detached direct numerical simulations of turbulent two-phase bubbly channel flow, Int. J. Multiphase Flow **37**, 647 (2011).
[17] I. Roghair, J. M. Mercado, M. Van Sint Annaland, H. Kuipers, C. Sun, and D. Lohse, Energy spectra and bubble velocity distributions in pseudo-turbulence: Numerical simulations vs. experiments, Int. J. Multiphase Flow **37**, 1093 (2011).
[18] S. Dabiri, J. Lu, and G. Tryggvason, Transition between regimes of a vertical channel bubbly upflow due to bubble deformability, Phys. Fluids **25**, 102110 (2013).
[19] J. Lu and G. Tryggvason, Dynamics of nearly spherical bubbles in a turbulent channel upflow, J. Fluid Mech. **732**, 166 (2013).
[20] M. Ilić, Statistical analysis of liquid phase turbulence based on direct numerical simulations of bubbly flows, Ph.D. thesis, Forschungszentrum Karlsruhe, 2006.
[21] S. Erdogan and M. Wörner, Analysis and modeling of liquid phase turbulence kinetic energy equation in bubbly flows via direct numerical simulation, Proceedings of the 2nd International Symposium on Multiscale Multiphase Process Engineering, Hamburg, 2014.
[22] C. Santarelli and J. Fröhlich, Direct numerical simulations of spherical bubbles in vertical turbulent channel flow, Int. J. Multiphase Flow **75**, 174 (2015).
[23] C. Santarelli and J. Fröhlich, Direct numerical simulations of spherical bubbles in vertical turbulent channel flow. Influence of bubble size and bidispersity, Int. J. Multiphase Flow **81**, 27 (2016).
[24] C. Santarelli, J. Roussel, and J. Fröhlich, Budget analysis of the turbulent kinetic energy for bubbly flow in a vertical channel, Chem. Eng. Sci. **141**, 46 (2016).
[25] P. Ern, F. Risso, D. Fabre, and J. Magnaudet, Wake-induced oscillatory paths of bodies freely rising or falling in fluids, Annu. Rev. Fluid Mech. **44**, 97121 (2012).
[26] M. Lance and J. Bataille, Turbulence in the liquid phase of a uniform bubbly air-water flow, J. Fluid Mech. **222**, 95 (1991).
[27] J. Martínez Mercado, D. Chehata Gómez, D. van Gils, C. Sun, and D. Lohse, On bubble clustering and energy spectra in pseudo-turbulence, J. Fluid Mech. **650**, 287 (2010).
[28] J. Rensen, S. Luther, and D. Lohse, The effect of bubbles on developed turbulence, J. Fluid Mech. **538**, 153 (2005).
[29] G. Riboux, F. Risso, and D. Legendre, Experimental characterization of the agitation generated by bubbles rising at high Reynolds number, J. Fluid Mech. **643**, 509 (2010).
[30] S. Mendez-Diaz, J. C. Serrano-García, R. Zenit, and J. A. Hernández-Cordero, Power spectral distributions of pseudo-turbulent bubbly flows, Phys. Fluids **25**, 043303 (2013).
[31] E. Bouche, V. Roig, F. Risso, and A. M. Billet, Homogeneous swarm of high-Reynolds-number bubbles rising within a thin gap. Part 2. Liquid dynamics, J. Fluid Mech. **758**, 508 (2014).
[32] V. N. Prakash, J. M. Mercado, L. van Wijngaarden, E. Mancilla, Y. Tagawa, D. Lohse, and C. Sun, Energy spectra in turbulent bubbly flows, J. Fluid Mech. **791**, 174 (2016).
[33] R. O. Fox, On multiphase turbulence models for collisional fluid-particle flows, J. Fluid Mech. **742**, 368 (2014).
[34] T. R. Auton, The lift force on a spherical body in a rotational flow, J. Fluid Mech. **183**, 199 (1987).
[35] S. P. Antal, R. T. Lahey, and J. E. Flaherty, Analysis of phase distribution in fully developed laminar bubbly two-phase flow, Int. J. Multiphase Flow **17**, 635 (1991).
[36] A. Burns, T. Frank, I. Hamill, and J.-M. Shi, The Favre averaged drag model for turbulent dispersion in Eulerian multi-phase flows, Proceedings of the 5th International Conference on Multiphase Flow, Yokohama, 2004, paper 392.
[37] S. B. Pope, *Turbulent Flows*, 1st ed. (Cambridge University Press, Cambridge, 2000).
[38] F. R. Menter, Two-equation eddy-viscosity turbulence models for engineering applications, AIAA J. **32**, 1598 (1994).
[39] T. Ma, A contribution to turbulence modeling in bubbly flows, Ph.D. thesis, Technische Universität Dresden, 2017.
[40] A. Prosperetti (private communication).